

Designing Practical Motions for Autonomous Underwater Vehicles: A Ship Hull Survey Mission

R.N. Smith ^{*,1}

*Robotic Embedded Systems Laboratory, Department of Computer Science,
University of Southern California, Los Angeles, CA 90089, USA*

M. Chyba, S.B. Singh ¹

*Mathematics Department, College of Natural Sciences,
University of Hawai'i, Honolulu, HI 96822, USA*

S.K. Choi, G. Marani ²

*Autonomous Systems Laboratory, College of Engineering,
University of Hawai'i, Honolulu, HI 96822, USA*

Abstract

The primary focus of this paper is to provide a solution to the practical motion planning problem of a ship hull survey to be performed by an Autonomous Underwater Vehicle (AUV). In particular, we examine the bulbous bow portion of the hull and present a reasonable survey strategy. Unique to this applied study, is the approach to the problem via differential geometric techniques. The motion planning problem is solved by use of a geometric reduction to the dynamic equations of motion, and the trajectory is generated through the concatenation of kinematic motions. The control strategy for each arc of the trajectory is calculated and implemented onto a test-bed vehicle. Experimental results are presented to demonstrate the effectiveness of this motion planning solution.

Key words: Applied Motion Planning, Kinematic Motion, Autonomous Underwater Vehicle, Experimental Validation, Ship Hull Survey, Bulbous Bow

^{*} Corresponding author.

Email address: ryannsmi@usc.edu (R.N. Smith).

¹ This research is supported in part by the National Science Foundation grant DMS-0608583

² This research is supported in part by the Office of Naval Research grants N00014-03-1-0969, N00014-04-1-0751 and N00014-04-1-0751

1 Introduction

Approximately 90% of the goods traded throughout the world are carried by the international shipping industry. What many consider to be a normal life, would not be possible without maritime shipping. With incentives of competitive freight costs during a time of increasing fuel expenses, seaborne trade continues to expand. Thus, prospects for the maritime industry's further growth continues to be strong. Currently, there are more than 50,000 merchant ships trading internationally and transporting many different types of cargo. This fleet belongs to more than 150 nations, and employs over a million seafarers.

With a high volume of ships arriving from worldwide destinations, it is of utmost importance to monitor and protect the ports which are so crucial to a country's trading market. To this end, it has become an interest of homeland security and port authorities to examine the hulls of ships before they enter port. This problem has attracted much research interest in the Autonomous Underwater Vehicle (AUV) and ocean engineering community and is currently still under much investigation. We do not propose to entirely solve the matter here, but offer a solution to a motion planning problem motivated from ship hull inspections.

Many of the large vessels which would require examination before entering a port have a bulbous bow. An example of such can be seen on the USS George H.W. Bush (CVN 77) shown in Fig. 1. This bulb is positioned to sit just below the design water line and has the purpose of reducing the height of the bow wake of the vessel which in turn reduces the hull drag which implies better efficiency. Bulbs come in all different shapes and sizes and are optimized for a given ship design. Such a feature provides an interesting control theory problem for which to consider motion planning and trajectory design.



Fig. 1. USS George H.W. Bush (CVN 77), GlobalSecurity.org (2008).

In this paper, we approach the motion planning problem and control strategy design by use of the architecture of differential geometry. This framework provides the structure necessary to consider an agile AUV that can move in all six degrees-of-freedom (DOF). Additionally, this framework includes a straightforward method to accommodate under-actuated scenarios, such as thruster failure or considering a standard torpedo-shaped vehicle. Recent research has shown that such geometric methods can be used to design implementable control strategies for AUVs, and is an effective method for solving the motion planning problem, c.f., Smith (2008).

We begin by developing the equations of motion for the submerged rigid body in a traditional manner, followed by the same equations presented in the language of differential geometry. We include a short section to motivate the use of this geometric architecture and give a literature review of similar research. Section 4 describes the design and calculation of the control strategies and includes the actual controls to be implemented onto a test-bed vehicle. The implementation of the calculated control strategies are carried out on the Omni-Directional Intelligent Navigator (ODIN), which is owned and maintained by the Autonomous Systems Laboratory, College of Engineering, University of Hawaii. Experimental results from these tests are presented in Section 5, which also includes analysis of these implementations. We conclude this paper with an overall assessment and provide ideas for future research.

2 Equations of Motion

In this section, we present a working model for the kinematics and dynamics of a submerged, three-dimensional rigid body that can move in six degrees-of-freedom. These equations assume that the body is submerged in a viscous fluid and incorporate the forces and moments arising from added mass, hydrodynamic damping, gravity and buoyancy.

A derivation of the general rigid body equations of motion can be found in a classical mechanics text such as Lamb (1961), Meriam and Kraige (1997) or Ardema (2005). The addition of the hydrodynamic forces and moments into these general equations can be found in Lamb (1945) (see also Fossen, 1994), with an in-depth treatment of the hydrodynamic topics presented in Newman (1977).

In the sequel, we will use methods from geometric control theory to design the control strategies to be implemented onto the test-bed vehicle. To this end, we consider the equations of motion for the submerged rigid body expressed by use of the language of differential geometry. Since a derivation of these geometric equations would require an extensive background of language and notation which is beyond the scope of this paper, we refer the reader to Smith (2008) for a detailed derivation of both the classical equations and those derived by use of the geometric control framework.

2.1 Preliminary Kinematics

For the analysis of AUVs, it is necessary to work with two right-handed, orthogonal coordinate systems. We first need a reference frame from which to measure distances and angles. This is done by choosing an earth-fixed reference frame. For low-speed marine vehicles such as those studied here, the Earth's movement has a negligible effect on the dynamics of the vehicle. Thus, the earth-fixed frame may be considered as an inertial frame. To precisely identify the configuration of a rigid body, we need to know the position and orientation of a point on the body with

respect to the inertial reference frame. Thus, we will define a reference frame fixed to a chosen point on the body. These two reference frames are described in detail below.

The inertial frame is a right-handed, non-rotating, orthogonal reference frame and is taken to be earth fixed with accelerations neglected. This coordinate system $\Sigma_I : (O_I, \{s_1, s_2, s_3\})$ is defined with the s_1 and s_2 axes lying in the horizontal plane perpendicular to the direction of gravity, while the s_3 axis is orthogonal to the $s_1 - s_2$ plane and taken to be positive in the direction of gravity. We may also refer to this frame as the spatial reference frame. This choice of inertial reference frame is consistent with current oceanography and AUV literature. With this choice of coordinates, we get a reference frame positioned at the free surface ($s_3 = 0$) and s_3 corresponds to depth. Since we are considering an unbounded fluid domain, we may select an arbitrary position for the inertial frame, preferably in a location such that the depth of the vehicle is non-negative. The inertial frame is shown in Fig. 2.

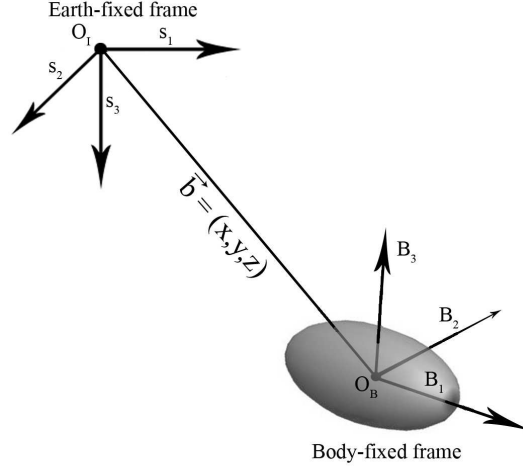


Fig. 2. Earth-fixed and body-fixed coordinate reference frames.

The body-fixed frame, shown in Fig. 2, is a right-handed, orthogonal reference frame which is fixed to a point on the body. This coordinate system $\Sigma_B : (O_B, \{B_1, B_2, B_3\})$ is defined with O_B located at a chosen point and the body axes B_1, B_2 and B_3 coincide with the principle axes of inertia:

- B_1 - longitudinal axis (positive to fore)
- B_2 - transverse axis (positive to starboard)
- B_3 - normal axis (positive to the keel)

The above definitions of reference frames suggests that the position and orientation of the vehicle be expressed relative to the spatial frame while the linear and angular velocities are defined relative to the body-fixed frame. Standard notation for these quantities are defined in SNAME (1950) and are reproduced in Table 1.

As seen in Fig. 2, we let $\mathbf{b} = (x, y, z)$ be the vector from the origin of the inertial frame to the origin of the body-fixed frame. The angular orientation of the body with respect to the earth-fixed frame can either be given using Euler angles or quaternions. In this dissertation, we choose to work with the Euler angles, accepting

DOF	Forces & Moments	Linear & angular velocity (body-fixed frame)	Positions & Euler angles
Surge	X	u	x
Sway	Y	v	y
Heave	Z	w	z
Roll	K	p	ϕ
Pitch	M	q	θ
Yaw	N	r	ψ

Table 1
SNAME notation for the study of underwater vehicles.

the fact that we may need two representations to fully avoid singularities.

Now, the configuration of a rigid body in six DOF can be described using $\boldsymbol{\eta} = (x, y, z, \phi, \theta, \psi)^t = (\mathbf{b}, \phi, \theta, \psi)^t = (\mathbf{b}, \boldsymbol{\eta}_2)^t$, where $\boldsymbol{\eta}_2 = (\phi, \theta, \psi)$ is the orientation of the body, relative to the spatial frame. In the body-fixed frame, $\boldsymbol{\nu} = (u, v, w)^t$ is the linear velocity, $\boldsymbol{\Omega} = (p, q, r)^t$ is the angular velocity, $\boldsymbol{\varphi}_\nu = (X, Y, Z)^t$ represents the external control forces and $\boldsymbol{\tau}_\Omega = (K, M, N)^t$ represents the external control moments. The external control forces and moments are applied by the actuators on the vehicle and can be represented collectively as the vector $\boldsymbol{\sigma} = (\boldsymbol{\varphi}_\nu, \boldsymbol{\tau}_\Omega)^t = (X, Y, Z, K, M, N)^t$.

2.2 Dynamic Equations of Motion

Following SNAME (1950), we express the submerged weight of the vehicle as $W = mg$ and the buoyancy force as $B = \rho g \mathcal{V}$, where ρ is the fluid density, g is the gravitational acceleration, m is the mass of the vehicle and \mathcal{V} is the submerged volume of the fluid displaced by the vehicle³. Suppose that the gravitational force acts through the center of gravity $\mathbf{C}_G = (x_G, y_G, z_G)$ and the buoyancy force acts through the center of buoyancy ($\mathbf{C}_B = (x_B, y_B, z_B)$). Then, we present the equations of motion for a rigid body submerged in a viscous fluid in the following Lemma.

Lemma 1 *The equations of motion of a rigid body moving in six degrees of freedom submerged in a viscous fluid and subject to the restoring forces and moments of*

³ Here we choose to denote the submerged volume as \mathcal{V} rather than the conventional ∇ since ∇ will be used to represent a differential geometric object called an affine connection.

gravity and buoyancy are given by:

$$\begin{pmatrix} m\mathbb{I}_3 + M_f & 0_{3 \times 3} \\ 0_{3 \times 3} & J_b + J_f \end{pmatrix} \begin{pmatrix} \dot{\mathbf{v}} \\ \dot{\boldsymbol{\Omega}} \end{pmatrix} - D(\mathbf{v})\mathbf{v} - Cor_B(\mathbf{v})\mathbf{v} + g(\boldsymbol{\eta}) = \boldsymbol{\sigma}(t), \quad (1)$$

where

$$g(\boldsymbol{\eta}) = \begin{bmatrix} (W - B) \sin \theta \\ -(W - B) \cos \theta \sin \phi \\ -(W - B) \cos \theta \cos \phi \\ -(y_G W - y_B B) \cos \theta \cos \phi + (z_G W - z_B B) \cos \theta \sin \phi \\ (z_G W - z_B B) \sin \theta + (x_G W - x_B B) \cos \theta \cos \phi \\ -(x_G W - x_B B) \cos \theta \sin \phi - (y_G W - y_B B) \sin \theta \end{bmatrix}, \quad (2)$$

$\begin{pmatrix} m\mathbb{I}_3 + M_f & 0_{3 \times 3} \\ 0_{3 \times 3} & J_b + J_f \end{pmatrix}$ is the added mass matrix, $D(\mathbf{v})$ is a diagonal matrix representing the linear and quadratic viscous damping terms and is given by $D(\mathbf{v}) = \text{diag}(D_1|u|, D_2|v|, D_3|w|, D_4|p|, D_5|q|, D_6|r|)$, $Cor_B(\mathbf{v})$ is a matrix accounting for the Coriolis and centripetal forces, $\boldsymbol{\sigma}(t)$ accounts for the control forces and moments.

Rewriting these equations in the standard Newton-Euler notation ($F=ma$) and separating translational and rotational motion results in the following equivalent expressions:

$$M\dot{\boldsymbol{\nu}} = -\boldsymbol{\Omega} \times M\boldsymbol{\nu} + D_{\boldsymbol{\nu}}(\boldsymbol{\nu})\boldsymbol{\nu} - g(\mathbf{b}) + \boldsymbol{\varphi}_{\boldsymbol{\nu}} \quad (3)$$

$$J\dot{\boldsymbol{\Omega}} = -\boldsymbol{\Omega} \times J\boldsymbol{\Omega} - \boldsymbol{\nu} \times M\boldsymbol{\nu} + D_{\boldsymbol{\Omega}}(\boldsymbol{\Omega})\boldsymbol{\Omega} - g(\boldsymbol{\eta}_2) + \boldsymbol{\tau}_{\boldsymbol{\Omega}}, \quad (4)$$

where $M\boldsymbol{\nu} \times \boldsymbol{\Omega}$ and $J\boldsymbol{\Omega} \times \boldsymbol{\Omega}$ account for the Coriolis and centripetal forces. Note that $\boldsymbol{\varphi}_{\boldsymbol{\nu}}$ and $\boldsymbol{\tau}_{\boldsymbol{\Omega}}$ now only include the external control forces acting on the submerged rigid body.

This concludes a typical derivation of the general equations of motion for a submerged rigid body in a viscous fluid. In Smith (2008), it is shown that these well-known equations of motion (see e.g., Fossen (1994)) are equivalent to a *forced affine connection control system* on a differentiable manifold. In the sequel, we follow this differential geometric control theory approach to provide solutions to the motion planning problem for the submerged rigid body. Thus, we present the equations of motion for the submerged rigid body, expressed as a forced affine connection control system, in the following Lemma.

Lemma 2 *Let $Q = \text{SE}(3)$ be the differentiable manifold referred to as the configuration manifold, $\widetilde{\nabla}$ be the modified Levi-Civita connection on Q associated with the*

Riemannian metric $\mathbb{G} = \begin{pmatrix} M & 0 \\ 0 & J \end{pmatrix}$, and let the set of input control vector fields for

the rigid body be given by $\mathcal{I} = \{\mathbb{I}_1^{-1}, \dots, \mathbb{I}_6^{-1}\}$. Let $G^\# P(\gamma(t))$ represent the restoring forces arising from gravity and buoyancy. Then, the equations of motion of a rigid body submerged in a viscous fluid are given by the forced affine connection control system:

$$\widetilde{\nabla}_{\gamma'} \gamma' = \mathbb{G}^\# P(\gamma(t)) + \sum_{i=1}^6 \mathbb{I}_i^{-1}(\gamma(t)) \sigma^i(t), \quad (5)$$

where $\boldsymbol{\sigma}(t) = (\sigma^1(t), \sigma^2(t), \dots, \sigma^6(t))^t = (X, Y, Z, K, M, N)^t$ represents the controls.

We present Lemma 2 without proof since the differential geometry background and the required tools are lengthy to define and out of the scope of this paper. Also, in the following sections, we will not explicitly refer to the geometric objects mentioned in Lemma 2, we only present these differential geometric equations of motion as a means of completeness, as these are from which the vehicle controls are calculated. For a proof of Lemma 2, we refer the interested reader to Smith (2008). This publication, and the references contained therein, provide complete details on the submerged rigid body expressed in the context of differential geometric control theory.

3 Motivation and Application

Recent research has shown that geometric control theory is a useful and effective way to design and calculate control strategies for many simple mechanical systems, including the submerged rigid body (e.g., Leonard and Krishnaprasad (1995), Leonard (1995), Bullo et al. (2000), Bullo and Lynch (2001), Bullo (2004) and Bullo and Lewis (2005)). The submerged rigid body in an ideal fluid is treated as an example in the later four references. These geometric techniques have been extended to include viscous damping and restoration forces and moments experienced by a rigid body submerged in a viscous fluid with $C_B \neq C_G$ in a series of papers, Chyba and Smith (2008), Smith et al. (2008), Smith et al. (2009) and Smith (2008). In these recent publications, the authors describe a few simple scenarios which might be experienced by an AUV in operation, and provide some solutions to the particular motion planning problems. In this paper, we provide a more in-depth analysis of one of the operational tasks proposed. In particular, we consider a more in-depth examination of Mission 7 from Smith (2008); surveying the bulbous bow of a ship.

As previously mentioned, there has been a growing interest in the inspection of

ship hulls as well as port facilities. These tasks are physically intensive and require the involvement of highly-skilled human divers. Such labor intensive work comes with a potential risk to the diver. These risks are exponentially increased in the case when hazardous foreign elements, such as explosives, are present. In an effort to reduce the risk to human life, the use of Remotely Operated Vehicles (ROVs) are being called upon for this task. However, this procedure also requires intense human involvement for safely piloting the vehicle around the ship. Moreover, both of these methods do not guarantee 100% coverage, as the area around a ship in berth can be highly confined and cluttered. Operation of a tethered vehicle in these confines makes it even more difficult to perform the task successfully.

Due to ever pressing military reasons, engineers have been working on automating this process. By use of an AUV, we can reduce the risk to human life and additionally provide around-the-clock surveillance of ships and port facilities. With this as motivation, we propose to apply geometric control theory to design implementable trajectories which control an AUV on a path to survey a portion of the hull or harbor structure.

Our choice of surveying the bulbous bow provides an interesting practical problem in many ways. First, due to its peculiar shape it is a challenging control problem from a geometrical point of view. Secondly, in rough water the body of the bulb is subjected to an alternating inflow velocity field, preventing the development of stable destructive wave interference. Based on this type, as well as others types of hydrodynamic forces faced by the bulb, it is imperative to take added care in its inspection and maintenance. Additionally, the problem of ship-dock structure damage has existed since the primitive docks were constructed. Large ships having bulbous bows are an added factor for such structure damage. Hence, we consider it imperative to have the ability to effectively survey the bulbous bow.

Since the shape of the bulb affects the performance of the vessel at sea, each bulb is uniquely constructed for an individual ship and many different shapes and sizes can be seen in use today. However, from a designers point of view, the bulb can essentially be approximated by a cylindrical solid capped with a hemisphere. This is the simplified scenario that we assume for our experiments. Small alterations in the shape of the bulb will not greatly affect the design of our trajectories. Additionally, for very unique bulb shapes, similar methods to those described in the sequel can be used to design trajectories which better fit those protrusions. Figure 3 displays a typical bulbous bow along with its dimensions.

4 Control Strategy

The control strategy presented here was designed by following the procedure outlined in Chapter 4 of Smith (2008), and then adapting it for implementation onto the considered test-bed vehicle as described in Chapter 5 of the same reference. To summarize this procedure, we begin by first applying a geometric reduction pro-

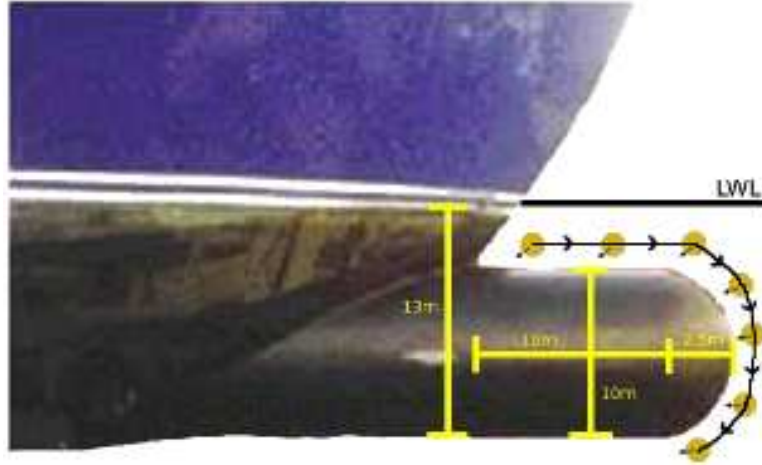


Fig. 3. This is a graph of the overall motion shown with a bulbous bow image.

cedure to the dynamic system (acceleration control inputs) described by Eqns. (5), and then calculating the decoupling vector fields for the kinematic system (velocity control inputs). A decoupling vector field is a vector field whose integral curves (under any reparameterization) are solutions to the kinematic system as well as the dynamic system. In particular, the integral curves of the decoupling vector fields define trajectories for the kinematic system that can be extended to realizable trajectories of the dynamic system. Thus, we are able to solve the motion planning problem for the kinematic system by the use of decoupling vector fields, and this solution can be extended to a solution for the dynamic system. For the scenario presented here, the pure motions (surge, sway heave, roll, pitch and yaw) from the point-of-view of the body-fixed reference frame are some examples of integral curves of decoupling vector fields. Other examples can be calculated as linear combinations of the pure motions. The decoupling vector fields for the fully-actuated scenario assumed here, as well as many under-actuated scenarios for ODIN are calculated and presented in Chyba et al. (2009a).

This geometric reduction technique is similar to solving a second-order differential equation by substitution of variables. Although this method does not find *all* solutions to the motion planning problem for the dynamic system, we are able to calculate some solutions without explicitly solving the complete dynamic system. Once we have chosen the integral curves of the decoupling vector fields that connect the initial and final configurations, we reparameterize and concatenate them to define the trajectory that we would like the vehicle to follow. The control strategy is calculated via inverse kinematics by applying Theorem 13.2 in Bullo and Lewis (2005) and the extension of this result presented in Smith (2008). For implementation onto the test-bed vehicle, the calculated control strategy must be converted to a piece-wise constant function with respect to time. This restriction is based upon characteristics of the chosen test-bed vehicle. In particular, we must account for the refresh rate of the actuator controller, and make a conscious effort to keep the thrusters operating in a steady state, which reduces their transient output re-

response. Since we are implementing in full open-loop, we try to reduce potential errors wherever possible. In the sequel, we present the calculated control strategies in the piece-wise constant structure, since the focus of this paper is driven by the implementation results and not the specific control design.

As previously mentioned, we implemented the calculated control strategies onto the agile and fully-actuated AUV, ODIN, which is shown in Fig. 4. Complete details and specifications for this vehicle can be found in Chyba et al. (2006) or Chyba et al. (2008), with specifics on implementation criteria contained in Smith (2008). ODIN's main body is a 0.64 m diameter sphere made of anodized aluminum (AL 6061-T6). Eight Tecnydyne brushless thrusters are attached to the sphere via four fabricated mounts, each holding two thrusters. These thrusters are evenly distributed around the sphere with four oriented vertically and four oriented horizontally. This design provides instantaneous and unbiased motion in all six DOF, contrary to the more common torpedo-shaped vehicles. Unique to ODIN's construction is the control from an eight dimensional thrust to move in six DOF. To calculate the six-dimensional thrust σ resulting from the eight-dimensional thrust ζ (from the thrusters), or vice-versa, we apply a linear transformation to ζ . We omit the details of this transformation here, but refer the interested reader to Smith (2008) or Chyba et al. (2009b).

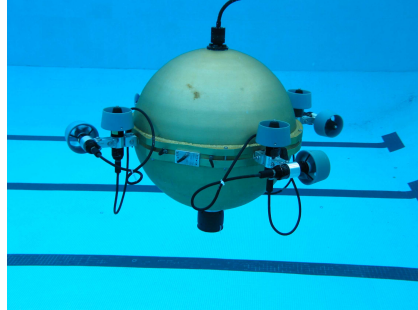


Fig. 4. ODIN operating in the pool.

Fully assembled, ODIN's mass is 123.8 kg and she is positively buoyant by 1.3 N. ODIN is depth rated for 100 meters. The numerical values of additional various parameters used for modeling ODIN are given in Table 2. These values were derived from estimations and experiments performed on ODIN. The added mass terms ($M_f^u, M_f^v, M_f^w, J_f^p, J_f^q, J_f^r$) were estimated from formulas found in Allmendinger (1990) and Imlay (1961). Moments of inertia (I_{xx}, I_{yy}, I_{zz}) were calculated using experiments outlined in Bhattacharyya (1978). We used inclining experiments to locate C_G , which we take as the center of our body-fixed reference frame (i.e., $C_G = O_B$). Due to the symmetry of the vehicle, the center of buoyancy C_B , is assumed to be the center of the spherical body of ODIN. The location of C_B is measured from $C_G = O_B$, and is given in Table 2.

Major internal components include a pressure sensor, inertial measurement unit, leakage sensor, heat sensor and 24 batteries (20 for the thrusters and four for the CPU). ODIN is able to compute and communicate real time, yaw, pitch, roll, and depth and can run autonomously for up to five hours from either a tethered or fully-autonomous mode.

ODIN does not have real time sensors to detect horizontal ($x - y$) position. Instead,

Mass	123.8 kg	$B = \rho g \mathcal{V}$	1215.8 N	C_B	(0, 0, -7) mm
Diameter	0.64 m	$W = mg$	1214.5 N	C_G	(0, 0, 0) mm
M_f^u	70 kg	M_f^v	70 kg	M_f^w	70 kg
I_{xx}	5.46 kg m ²	I_{yy}	5.29 kg m ²	I_{zz}	5.72 kg m ²
J_f^p	0 kg m ²	J_f^q	0 kg m ²	J_f^r	0 kg m ²

Table 2

Main dimensions and hydrodynamic parameters for ODIN.

experiments are videotaped from a platform 10m above the water’s surface, giving us a near nadir view of ODIN’s movements. Videos are saved and horizontal position data are post-processed for later analysis. A real-time system utilizing sonar was available on ODIN, but was abandoned for two main reasons. First, the sonar created too much noise in the diving well and led to inaccuracies. More significantly, in the implementation of our control strategies, ODIN is often required to achieve large ($> 15^\circ$) list angles which render the sonars useless for horizontal position. Many alternative solutions were attempted and video provided a cost-effective solution which produced accurate results. We are able to determine ODIN’s relative position in the testing pool to ± 10 cm.

Along with the tests to determine the values in Table 2, we also tested the thrusters. Each thruster has a unique voltage input to power output relationship. This relationship is highly nonlinear and is approximated using a piecewise linear function which we refer to as our thruster model. More information regarding the thruster modeling can be found in Smith (2008). For the application described here, we additionally assume that ODIN has a forward facing camera (or other data collecting sensor) mounted at the equator of the spherical hull.

The intention of this paper is to present implementation results of geometrically designed control strategies to survey the bulbous bow of a ship. Figure 3 displays a side view of a typical bulb along with the dimensions considered here. To survey this uniquely-shaped object, we propose two separate trajectories. The first is a semi-circular trajectory as depicted in Figure 5. Here, the vehicle performs a pure heave while simultaneously applying a pure surge. This trajectory can be used to survey the front of the bulb (e.g., as depicted in Fig. 3) or to perform repeated transects up and down the longitudinal axis of the bulb as shown in Fig. 6.

The second trajectory considered to survey a bulbous bow is a motion parallel to the free surface while maintaining a desired pitch angle to point the camera, or sensor, at the surface of the bulb. This trajectory is depicted by the line parallel to the load water line (LWL) in Fig. 3. We now continue by presenting the control strategies for both of these scenarios, along with a third strategy which is the modified concatenation of the two previously mentioned.



Fig. 5. Side view of a bulbous bow on a ship. Also pictures is the semi-circle trajectory for the inspection of the front of a bulbous bow.



Fig. 6. Front view of the bulbous bow of the M/V Eurodam. Also depicted is the trajectory to survey the sides of the bulb. Picture modified from Rijkaart (2008).

We remark that all control strategies presented here are designed such that the vehicle begins at the origin with zero velocity, and ends at η_f with zero velocity. When multiple trajectories are concatenated, each portion of the trajectory begins and ends with zero velocity. For details on the reparameterization technique used to ensure zero velocity states at the beginning and end of a trajectory, see Smith (2008).

Additionally, the implementation of the following control strategies is performed in the diving well at the Duke Kahanamoku Aquatic Complex at the University of Hawaii. As such, we are unable to perform trajectories that are full scale with respect to the dimensions shown in Fig. 3. We scale the height of the bulb from 10 m to 2.5 m, which implies that the 2.5 m radius of the hemisphere scales to approximately 0.5 m. For the motion parallel to the free surface, we scale the 10 m length of the bulb to 5 m.

4.1 Strategy One: Semi-circle

The first strategy we wish to construct is the semi-circle trajectory to inspect the front and the sides of the bulbous bow. This motion is constructed by simultaneously applying controls in both pure heave and pure surge. The pure heave control is designed so that the vehicle realizes a net 2.5 m pure heave. The surge control is designed such that the vehicle begins at rest, realizes a negative pure surge of 0.5 m, then moves 0.5 m in the positive surge direction to culminate with zero net movement in pure surge. The final configuration for the vehicle is $\eta_f = (0, 0, 2.5, 0, 0, 0)$ meters. We parameterize this motion to begin and end at rest, and based on the operational velocity of ODIN, the duration of the motion is 10.7 seconds. We present the calculated control strategy in Table 3 as a six-dimensional control, corresponding to the six DOF in the body-fixed reference frame. This six-dimensional control

is converted to an eight-dimensional control on-board ODIN to compute the prescribed controls sent to each of the eight thrusters.

Time (s)	Applied Thrust (6-dim.) (N)	Time (s)	Applied Thrust (6-dim.) (N)
0	(0,0,0,0,0,0)	6.5	(32.7, 0, 30.04, 0, 0, 0)
0.9	(-32.7, 0, 30.04, 0, 0, 0)	7.7	(32.7, 0, -24.56, 0, 0, 0)
2.8	(-32.7, 0, 30.04, 0, 0, 0)	8.6	(-30.99, 0, -24.56, 0, 0, 0)
3.7	(30.99, 0, 30.04, 0, 0, 0)	9.8	(-30.99, 0, -24.56, 0, 0, 0)
4.9	(30.99, 0, 30.04, 0, 0, 0)	10.7	(0,0,0,0,0,0)
5.8	(32.7, 0, 30.04, 0, 0, 0)		

Table 3
Piece-wise constant control strategy to perform a semi-circle trajectory.

4.2 Strategy Two: Horizontal Survey

This trajectory is similar to the Mission 5 strategy that is designed in Chapter 5.5.5 in Smith (2008). The author’s original intent was to design a control strategy for a seabed survey mission. Here, we use the same pitch angle of $\theta = -20^\circ$, but move in a negative surge direction rather than positive⁴. This control strategy provides the ability to survey the top of the bulb, while choosing $\theta = 20^\circ$ and moving in the positive surge direction will allow for survey of the bottom of the bulb. The basic idea for this control strategy is to pitch the vehicle so that the forward-looking camera points downward, then apply a pure surge control while maintaining the desired pitch angle to survey along top or bottom of the bulb. In this case, we prescribe a -5 m pure surge and a final configuration for the vehicle of $\eta_f = (-5, 0, 0, 0, -20^\circ, 0)$. The duration of this motion is 38.6 seconds. The six-dimensional control strategy is given as the piece-wise constant function with respect to time shown in Table 4.

4.3 Strategy Three: Concatenated Motion

Here, we combine the control strategies presented in Sections 4.1 and 4.2 into a single implementable trajectory. Since both of the previous strategies were designed to begin and end at rest, we can simply concatenate them together. The final configuration for this motion is $\eta_f = (-5, 0, 2.5, 0, 0, 0)$, which is realized over a duration of 49.3 seconds. The six-dimensional control strategy is given as the piece-wise constant function with respect to time shown in Table 5.

⁴ The pitch angle of -20° is chosen based on the physical limitations of the test-bed vehicle ODIN.

Time (s)	Applied Thrust (6-dim.) (N)	Time (s)	Applied Thrust (6-dim.) (N)
0	(0,0,0,0,0,0)	31.9	(-10.7, 0, 7.6, 0, -2.91, 0)
0.9	(0.45, 0, 1.2, 0, -2.91, 0)	32.8	(4.6, 0, 2.02, 0, -2.91, 0)
5.9	(0.45, 0, 1.2, 0, -2.91, 0)	37.7	(4.6, 0, 2.02, 0, -2.91, 0)
6.8	(-10.7, 0, 7.6, 0, -2.91, 0)	38.6	(0,0,0,0,0,0)

Table 4

Piece-wise constant control strategy to survey the top portion of the bulbous bow.

Time (s)	Applied Thrust (6-dim.) (N)	Time (s)	Applied Thrust (6-dim.) (N)
0	(0,0,0,0,0,0)	42.3	(30.99, 0, 30.04, 0, 0, 0)
0.9	(0.45, 0, 1.2, 0, -2.91, 0)	43.5	(30.99, 0, 30.04, 0, 0, 0)
5.9	(0.45, 0, 1.2, 0, -2.91, 0)	44.4	(32.7, 0, 30.04, 0, 0, 0)
6.8	(-10.7, 0, 7.6, 0, -2.91, 0)	45.1	(32.7, 0, 30.04, 0, 0, 0)
31.9	(-10.7, 0, 7.6, 0, -2.91, 0)	46	(32.7, 0, -24.56, 0, 0, 0)
32.8	(4.56, 0, 5.02, 0, -2.91, 0)	46.3	(32.7, 0, -24.56, 0, 0, 0)
37.7	(4.56, 0, 5.02, 0, -2.91, 0)	47.2	(-30.99, 0, -24.56, 0, 0, 0)
38.6	(-32.7, 0, 30.04, 0, 0, 0)	48.4	(-30.99, 0, -24.56, 0, 0, 0)
41.4	(-32.7, 0, 30.04, 0, 0, 0)	49.3	(0,0,0,0,0,0)

Table 5

Piece-wise constant control strategy for the concatenation of the two strategies presented in Sections 4.1 and 4.2.

Note that, for this strategy, we do not allow any time for the pitch angle to return to zero before beginning the second segment of the trajectory. This is done so that the vehicle will remain pitched for a short time while beginning the semi-circle motion. The result is a trajectory similar to that shown in Fig. 3 where the forward facing camera points nearly normal to the surface of the bulb for a short duration.

5 Experiments

In the following sections, we present experimental results for the implementations of the control strategies given in Sections 4.1, 4.2 and 4.3. The control strategies were implemented in a full open-loop fashion, thus there are no feedback controllers in operation. We choose to implement in this way to demonstrate the effectiveness of the technique used to design the control strategies. Practically speaking,

we do not intend to implement open-loop controls in the field. However, utilizing this geometric method for path planning and control synthesis, then implementing the calculated control along with a standard adaptive or feedback controller will result in an effective control system for AUVs to survey ship hulls, and in particular, bulbous bows of ships.

As previously mentioned, the following experiments were implemented onto the test-bed vehicle ODIN in the diving well at the Duke Kahanamoku Aquatic Complex at the University of Hawai‘i. Details regarding the implementation process and any specifics related to the facility can be found in Smith (2008). We remark that the initial configuration for each experiment is taken to be the origin, $\eta_{init} = (0, 0, 0, 0, 0, 0)$; this location is positioned 1.5 m below the free surface. For our experiments, positive surge is towards the bow of the vehicle, positive sway is to starboard and positive depth is taken downward in the direction of gravity.

5.1 Implementation One: Semi-circle

We present the implementation of the control strategy given in Section 4.1. The intent is to have the vehicle realize a 2.5 m dive while simultaneously moving in the surge direction. The combined motions create a semi-circular trajectory which can be used to inspect the front or sides of the bulbous bow.

Figure 7 displays the implementation results of the control strategy given in Table 3 executed by ODIN. The first column of plots in Fig. 7 give the pertinent control forces (in Newtons) and control moments (in Newton meters) that were applied by ODIN during the implementation. In the second and third columns, we present the evolution of the vehicle during the test. The solid (blue) line denotes the actual evolution of ODIN. The dash-dot (red) line represents the theoretical evolution of ODIN.

We first examine the controls applied during the experiment. Note that for X , the magnitude of the control does not quite match the value given in Table 3. This is a result of implementing a six-dimensional control strategy onto a vehicle that is driven by eight thrusters. The linear transformation applied to convert from six dimensions to eight dimensions, and vice-versa, has a nonzero null space. This means that there are infinitely many transformations which convert the controls. ODIN’s on-board computer chooses one of these transformations for its computations. More information regarding this transformation can be found in Smith (2008), with specific details related to ODIN found in Hanai et al. (2003). The small applied thrusts seen for σ^2 can also be attributed to this transformation.

Next, consider the evolution of ODIN during the experiment. The main intent of this strategy was to realize both heave and surge motions. For the surge motion, the experimental results match well with the theoretical trajectory. We see deviation between the actual and theoretical evolutions begin around $t = 4$ seconds. This occurs because ODIN did not reach the full 0.5 m displacement. The actual evo-

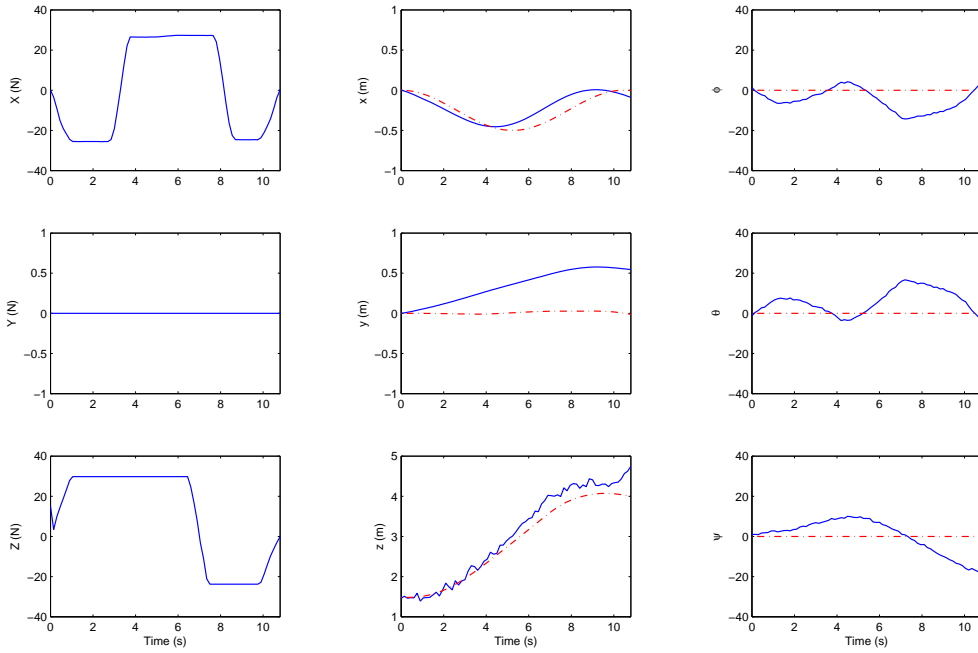


Fig. 7. Implementation One: Semi-circle trajectory. Solid (blue) line represents actual evolution, dash-dot (red) line represents the theoretical evolution.

lution is seen to be just out of phase of the theoretical prediction. This is probably a result of a small error in the drag coefficient calculated for ODIN. Overall, the surge motion was executed very well. Similarly for the heave motion, we see an excellent correspondence between theoretical predictions and experimental results. The sway motion displays a slight deviation that is a result of an initial yaw angle offset at the beginning of the experiment. Such an offset cannot be corrected since we are operating in open-loop. This type of implementation coupled with potential transient thruster response results in the discrepancies seen in the plots for the Euler angles. Such discrepancies are minimal and expected. Research is active in the design of a robust feedback controller for AUVs to track a given trajectory in the presence of initial disturbances such as yaw offsets and disturbance inputs. Initial results in this area can be found in Singh (2009) and Singh et al. (2009). It is an area of future work to implement such a controller onto ODIN for trajectory tracking experiments.

5.2 Implementation Two: Horizontal Survey

Figure 8 presents the experimental results for the implementation of the control strategy presented in Section 4.2. In this experiment, we are prescribing that the vehicle pitches to point the forward-looking camera downward, and then executes a 5 m path parallel to the free surface while maintaining a desired pitch angle and depth.

For this implementation, we had issues with initial yaw stabilization and frequently

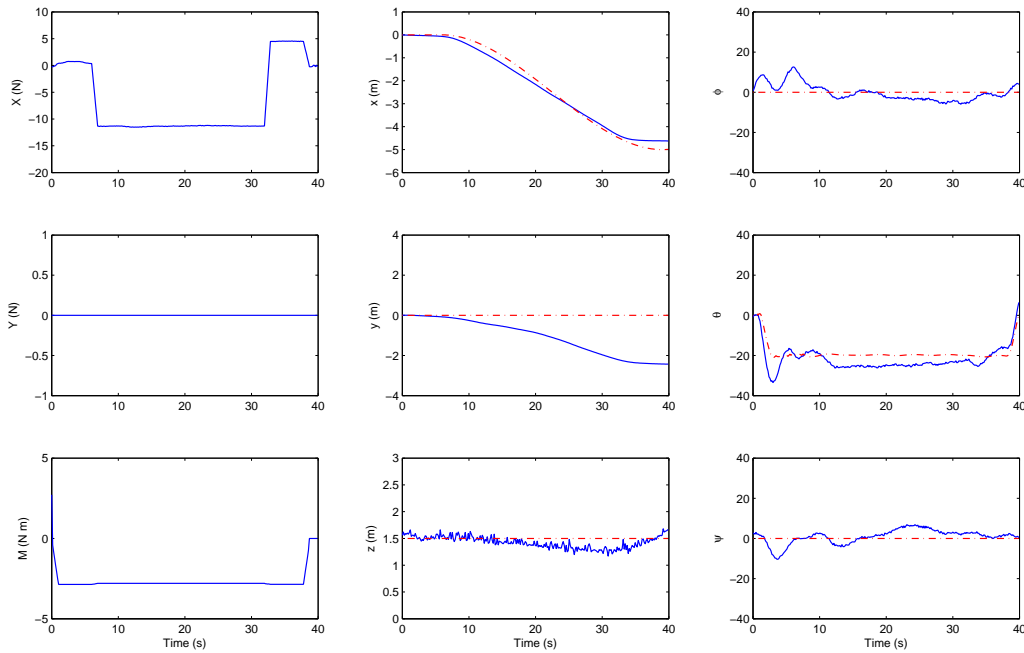


Fig. 8. Implementation Two: Horizontal survey. Solid (blue) line represents actual evolution, dash-dot (red) line represents the theoretical evolution.

had large offsets at the beginning of the trajectory. To compensate for this, we turned on a feedback controller for only the yaw control. ODIN has a Proportional-Derivative (PD) controller on-board, which can be activated to provide feedback in depth, roll, pitch and/or yaw.

The initial seven seconds of this strategy is devoted to stabilize the pitch angle to the prescribed -20° . During this time we see that the x , y and z evolutions remain stable with some disturbance seen in ϕ . The pitch angle did not quite stabilize during the initial seven seconds, but it quickly levels out from about $t = 12$ s onward. Note that this pitch angle is slightly more than the -20° prescribed. This excess pitch attributes to the slight rise to the surface seen in the depth evolution. Regardless, the actual depth evolution remains around the prescribed 1.5 m for the duration of the trajectory. For the surge evolution, we see that ODIN approximately realized the predicted 5 m displacement. Error here is again due to an error in the estimation of the drag coefficients for the vehicle. There is deviation in sway, which was a result of an initial yaw offset. Overall, the implementation of this control strategy matched well with the desired trajectory to be performed.

5.3 Implementation Three: Concatenated Motion

The experimental results displayed in Fig. 9 represent the concatenation of the two strategies presented in Sections 4.1 and 4.2. The overall trajectory that the vehicle is expected to perform is presented in Fig. 3. The idea is that the vehicle begins above the bulb and close to the bow of the ship, it pitches to point the camera downward,

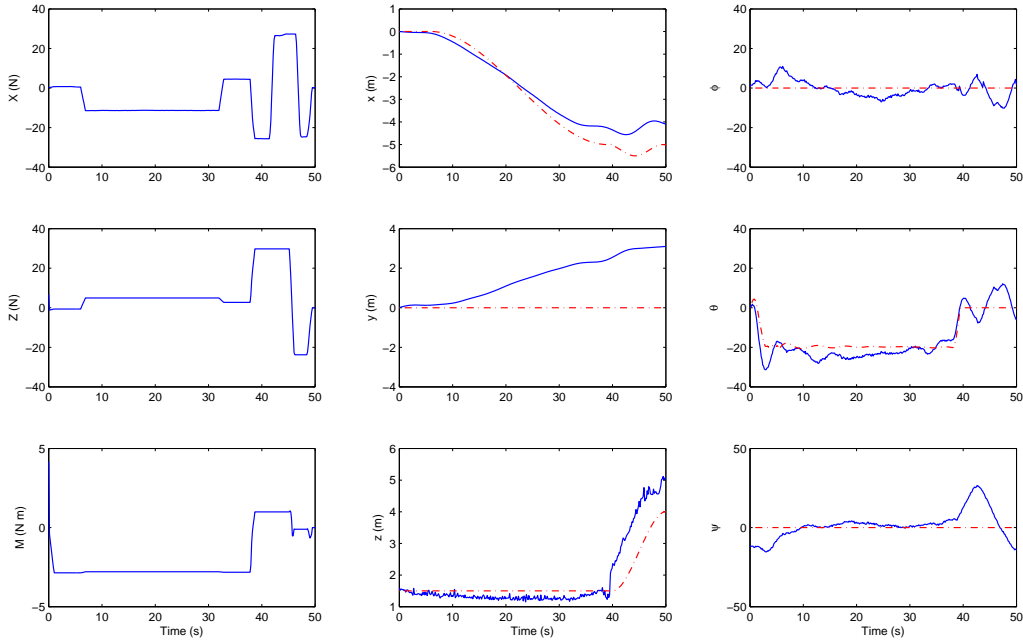


Fig. 9. Implementation Three: Concatenation of the semi-circle trajectory and the horizontal survey. Solid (blue) line represents actual evolution, dash-dot (red) line represents the theoretical evolution.

then traverses the length of the bulb parallel to the free surface. Upon reaching the end of the bulb, the AUV performs the semi-circle motion to examine the front portion of the bulb. For this concatenated strategy, we choose not to apply controls at the end of the initial segment to undo the prescribed pitch angle. This is done in an attempt to create the effect seen in Fig. 3, where the camera points nearly normal to the surface of the bulb for the first half of the semi-circle trajectory.

Note that the concatenation of two control strategies can give different results from those obtained by implementing each individually. This is directly related to the ability to stabilize the vehicle at the junction connecting the two strategies. Based upon the design of the control strategies, each segment of the concatenation should begin and end with zero velocity, thus making the concatenation feasible. However, this does not always occur in practice. In an effort to perform concatenated strategies well, we again activated a feedback controller for the yaw control for this experiment.

The initial 40 seconds of the implementation displayed in Fig. 9 is the strategy presented in Section 5.2, while the remainder of the experiment is the semi-circle strategy presented in Section 5.1. During the initial segment of the trajectory, we see similar results to those described in Section 5.2. The depth remains fairly constant at 1.5 m, the AUV realizes approximately 5 m in surge and the pitch angle is just less than the prescribed -20° . We also observe a sway deviation from an initial yaw offset.

Examining the remaining 20 seconds of the implemented strategy, we see behavior similar to that presented in Section 5.1, with the exception that the error from the first segment of the trajectory is introduced as the initial condition for the second leg of the concatenated motion. We see the initial negative surge of 0.5 m followed by a positive surge evolution of approximately 0.5 m, as prescribed. The depth evolution shows an overshoot in depth by about 1 m. The pitch evolution after 40 seconds oscillates about zero with a magnitude less than ten degrees. This is a result of not stabilizing the pitch angle to zero before beginning the semi-circle trajectory. Here, the vehicle is simply relying on the righting arm to return it to an upright position. The oscillations present in roll are an artifact of the small distance between the center of gravity and center of buoyancy, i.e., small righting arm. This configuration provides a very controllable vehicle in the sense that it can realize many configurations by use of the on-board thrusts, however this results in a decrease in stability of the AUV. Hence, reduced stability coupled with the open-loop implementation results in the expectation of small perturbations and oscillations in the evolution of the vehicle. The yaw evolution begins with an initial offset that is remedied within the first 10 seconds. Note that this deviation arises during the time that the pitch control is operating. At $t = 40$ s, we again notice a spike in the yaw, which corresponds to a time when the vehicle is releasing the pitch angle.

6 Conclusions

In this paper, we have presented the equations of motion governing the submerged rigid body in both a standard form as well as a form utilizing the architecture of differential geometry. By use of these geometric equations, we are able to provide solutions to the motion planning problem for AUVs via a geometric reduction and examination of the decoupling vector fields for the system. This geometric control theory technique has been proven to be an effective path planning tool for AUVs, especially those operating in an under-actuated condition, see e.g., Smith (2008) and Smith et al. (2009). Here, we considered a direct application of this path planning technique to examine the bulbous bow of ships.

Due to the unique shape and location, examination and survey of the bulbous bow provides an interesting motion planning problem for the submerged rigid body. We do not provide an exhaustive survey algorithm, but propose two control strategies which can be used to examine the majority of the bulb itself. For implementation purposes, the experiments presented here have been scaled down and assume a general form of the bulb. Trajectories to examine an actual bulbous bow of a ship would need to be generated for the specific size and shape of the bulb. The intent here is to present an application of an emerging technique in the area of motion planning for the submerged rigid body.

The experimental results presented here extend the work developed in Smith (2008), and further validate the design of implementable control strategies by use of differential geometric techniques. This architecture is not just a change of notation for

the same equations of motion, but a presentation with a much richer inherent structure. A structure which can be exploited for autonomous path planning in the event of a disabled vehicle (under-actuated) or used to guide the design of future AUVs. Research is currently ongoing to migrate the techniques presented here from the test-bed vehicle ODIN onto an AUV active in the open ocean. The ability to reproduce great implementation results such as those presented here gives us a good start to investigate the potential of actual sea trials.

The excellent correlation between theoretical predictions and experimental results shown in this paper are a result of working in a well-known and controlled environment. Many years and experimental trials have given us information on the specifics of the pool environment and we are able to limit uncertainties during the experiments. This will definitely not be the case in the ocean. To move from the pool to the ocean, significant adjustments will be necessary. First off, an AUV cannot operate strictly in an open-loop mode. Poorly known disturbance forces, such as ocean currents, are too large and unpredictable to be neglected or accounted for *a priori*. In an open-loop implementation in the ocean, we would expect to see large errors between theoretical predictions and experimental results.

A reasonable approach to begin the migration is to use our trajectories as the desired theoretical predictions, and implement a robust, feedback trajectory-tracking controller that can compensate for the external disturbances. Initial steps in this direction have been taken, and results can be found in Singh et al. (2009) and Sanyal and Chyba (2009). Once the theory contained in these references becomes well-developed and proven technology, we plan to implement a hybrid control scheme onto ODIN in the pool. We will begin with simple disturbances, such as initial deviations in the state of the vehicle. From the discussion presented in Sections 5.1-5.3, a known source of error comes from an initial offset in the vehicle's configuration, typically in yaw. Implementing a hybrid controller as previously described will require many upgrades to ODIN, or the use of an alternate AUV for sea trials.

This brings up the natural question regarding the applicability of the presented techniques to multiple types of underwater vehicles. First, the theoretical aspect, namely the geometric control, is independent of the choice of the vehicle. The geometric theory is solely based on the fact the underwater vehicle is an example of a simple mechanical control system; this is true for any underwater vehicle. Generalizing our work to alternate vehicle designs requires only slight modifications. If the vehicle has three planes of symmetry, which is common for AUVs, the basic foundations and formulations do not change. Obviously, the physical attributes, such as mass, inertia and added mass, need to be altered. This corresponds to the generation of a new kinetic energy metric for the kinematic reduction. Viscous drag coefficients need to be estimated for the specific vehicle, and the locations of the center of buoyancy and center of gravity need to be calculated to appropriately account for the restoration forces and moments. Aside from the obvious physical properties, the only major difference is changing the input control vector fields. These are the

basis upon which the decoupling vector fields, and hence the kinematic motions, are determined. This alteration is simply done by expressing the location and output of the actuators of the vehicle in the geometric formulation. In Smith (2008), the reader can find the generalization of the techniques presented here to two other underwater vehicles.

References

- Allmendinger, E. E., 1990. *Submersible Vehicle Design*. SNAME.
- Ardema, M. D., 2005. *Newton-Euler Dynamics*. Springer, New York.
- Bhattacharyya, R., 1978. *Dynamics of Marine Vehicles*. John Wiley & Sons.
- Bullo, F., 2004. Trajectory design for mechanical systems: From geometry to algorithms. *European Journal of Control* 10(5), 397–410.
- Bullo, F., Leonard, N., Lewis, A., 2000. Controllability and motion algorithms for underactuated lagrangian systems on lie groups. *Institute of Electrical and Electronics Engineers. Transactions on Automatic Control* 45(8), 1437–1454.
- Bullo, F., Lewis, A. D., 2005. *Geometric Control of Mechanical Systems*. Springer.
- Bullo, F., Lynch, K., 2001. Kinematic controllability for decoupled trajectory planning in underactuated mechanical systems. *IEEE Transactions. Robotics and Automation* 17 (4), 402–412.
- Chyba, M., Choi, S., Haberkorn, T., Smith, R. N., Zhao, S., 2006. Towards practical implementation of time optimal trajectories for underwater vehicles. In: *Proceedings of the 25th International Conference on Offshore Mechanics and Arctic Engineering*.
- Chyba, M., Haberkorn, T., Smith, R., Wilkens, G., 2009a. A geometrical analysis of trajectory design for underwater vehicles. *Discrete and Continuous Dynamical Systems-B* 11(2).
- Chyba, M., Haberkorn, T., Smith, R. N., Choi, S., 2008. Design and implementation of time efficient trajectories for an underwater vehicle. *Ocean Engineering* 35 (1), 63–76.
- Chyba, M., Haberkorn, T., Smith, R. N., Singh, S., Choi, S., 2009b. Increasing underwater vehicle autonomy by reducing energy consumption. *Ocean Engineering: Special Edition on AUVs* 36(1), 62–73.
- Chyba, M., Smith, R. N., 2008. A first extension of geometric control theory to underwater vehicles. In: *Proceedings of the 2008 IFAC Workshop on Navigation, Guidance and Control of Underwater Vehicles*. Killaloe, Ireland, Vol. 2, Part 1.
- Fossen, T. I., 1994. *Guidance and Control of Ocean Vehicles*. John Wiley & Sons.
- GlobalSecurity.org, 2008. USS George H.W. Bush. <http://www.globalsecurity.org/military/systems/ship/bulbous-bow.htm>, viewed May 2008.
- Hanai, A., Choi, H., Choi, S., Yuh, J., 2003. Minimum energy based fine motion control of underwater robots in the presence of thruster nonlinearity. In: *Proceedings of IEEE/RSJ International Conference on Intelligent Robots and Systems*. Las Vegas, Nevada, USA, pp. 559–564.

- Imlay, F., 1961. The complete expressions for added mass of a rigid body moving in an ideal fluid. Technical Report DTMB 1528, David Taylor Model Basin, Washington D.C.
- Lamb, H., 1945. Hydrodynamics, 6th Edition. Dover Publications.
- Lamb, H., 1961. Dynamics. University Press, Cambridge.
- Leonard, N., Krishnaprasad, P., 1995. Motion control of drift-free, left-invariant systems on lie groups. IEEE Transactions on Automatic Control 40(9), 1539–1554.
- Leonard, N. E., 1995. Periodic forcing, dynamics and control of underactuated spacecraft and underwater vehicles. In: Proceedings of the 34th IEEE Conference on Decision and Control. New Orleans, Louisiana, pp. 3980–3985.
- Meriam, J., Kraige, L., 1997. Engineering Mechanics, DYNAMICS, 4th Edition. John Wiley & Sons, Inc., New York.
- Newman, J., 1977. Marine Hydrodynamics. MIT Press, Cambridge, MA.
- Rijkaart, P., 2008. M/V Eurodam. <http://gcaptain.com/maritime/blog/tag/eurodam/>, viewed March 2009.
- Sanyal, A., Chyba, M., 2009. Robust feedback tracking of autonomous underwater vehicles with disturbance rejection. In: Proceedings of the American Control Conference (ACC). St. Louis, MO, to appear.
- Singh, S., Sanyal, A., Smith, R., Nordkvist, N., Chyba, M., 2009. Robust tracking control of autonomous underwater vehicles in presence of disturbance inputs. In: Proceedings of the 28th International Conference on Offshore Mechanics and Arctic Engineering (OMAE). Honolulu, Hawaii.
- Singh, S. B., 2009. Almost global feedback control of autonomous underwater vehicles. Master's thesis, University of Hawai'i at Manoa.
- Smith, R. N., 2008. Geometric control theory and its application to underwater vehicles. Ph.D. thesis, University of Hawai'i at Manoa.
- Smith, R. N., Chyba, M., Singh, S. B., 2008. Submerged rigid body subject to dissipative and potential forces. In: Proceedings of the IEEE Region 10 Colloquium and Third International Conference on Industrial and Information Systems. Kharagpur, India.
- Smith, R. N., Chyba, M., Wilkens, G. R., Catone, C. J., 2009. A geometrical approach to the motion planning problem for a submerged rigid body. International Journal of Control. Accepted, to appear.
- SNAME, 1950. Nomenclature for treating the motion of a submerged body through a fluid. Technical and Research Bulletin No. 1-5, The Society of Naval Architects and Marine Engineers.